JOURNAL OF MATERIALS SCIENCE 28 (1993) 691–699

Composition and precipitation inhomogeneities in melt-spun Al–Cu and Al–Zn ribbons

Q. LI, E. JOHNSON, A. JOHANSEN, L. SARHOLT-KRISTENSEN
Physics Laboratory, H.C. Ørsted Institute, University of Copenhagen, Universitetsparken 5, DK-2100 Copenhagen Ø, Denmark

Non-uniform distributions of solute content in the supersaturated α-Al matrix and inhomogeneous precipitation of metastable/stable phases have been studied in rapidly solidified Al–Cu and Al–Zn ribbons. Double-peaked X-ray diffraction lines from the α-Al matrix were observed in three as-quenched Al–Cu alloys and one annealed Al–Zn alloy. For as-quenched Al–Cu ribbons, variations in composition, microstructure and precipitate density across the ribbons result from local differences in cooling rates. These differences originate from recalescence during the solidification. The double-peaked diffraction lines for these alloys correspond to two compositions of the α-Al phase with less copper solute in the top-side than in the wheel-side of the ribbons. Subsequently, annealing of the samples leads to inhomogeneous precipitation of the metastable Θ′ phase across the whole thickness of the ribbons. Such inhomogeneities do not appear in as-quenched Al–Zn alloys which are quenched into a single α-Al phase. Splitting of the diffraction lines in the annealed ribbons arises from differences in the composition of two different α-Al matrix phases. The α-Al phase between the R phase lamellae has a low zinc content, while the α-Al phase where high densities of Guinier–Preston zones are retained has a higher zinc concentration.

1. Introduction

Although rapid solidification as compared with solid-state quenching can in general produce a more uniform and refined microstructure, the understanding of local inhomogeneities of the products during quenching and their influence on the subsequent precipitation processes is of technical importance. Jansen [1] initially proposed that the broadening of X-ray diffraction lines from a single α-Al phase within a particular Al–Cu eutectic foil may originate from a range of concentrations of the solute in supersaturated solution. In the α-Al phase of Al–Cu foils prepared by the gun technique, high-resolution electron microscopy combined with X-ray microanalysis gave evidence for compositional variations of up to 5 at % Cu in regions within a distance of 50–100 nm from grain boundaries [2]. Masur and Flemings [3] presented copper solute redistributions from 5.6 to 1.5 wt % in regions with an extent of 1400 nm near grain boundaries in the Al matrix for an Al–4.5 wt % Cu alloy. In addition, several investigations have been aimed at examining the overall compositional changes across the thickness of Al–Si and Al–Mg ribbons, without conclusive evidence for solute rejection [4, 5].

Heterogeneous microstructures have been observed in a number of rapidly solidified alloys [2, 6–9]. A typical example seen in cross-sections of the products is a refined grain zone at the chilling side followed by a columnar zone and a cellular zone at the top side. Such a morphological evolution of microstructure indicates that the crystallization starts with inhomogeneous nucleation, which may arise from locally different rates of solidification and simultaneous recalescence. Therefore, the precipitation behaviour of the alloys can be influenced during both quenching and annealing processes.

During the annealing of Al–Mg ribbons, van Mourik [10] observed a splitting of X-ray diffraction lines from the α-Al matrix. This phenomenon has also been reported in several other aluminium alloy systems [11–14]. Williams and Butler [15] proposed that the appearance of double-peaked diffraction lines from the α-Al matrix might be explained as a result of heterogeneous precipitation through a discontinuous reaction in regions adjacent to the grain boundaries. Alternatively, the appearance of two intensity maxima might be due to a compositional difference between regions near the grain boundaries and the bulk grains where the precipitation rates are non-uniform for the metastable phases [10]. In both cases, a precipitation-free zone would be expected along the grain boundaries. Unfortunately, no such evidence has been reported from microscopical investigations. It has also been proposed that elastic strains originating from the formation of coherent or semi-coherent precipitates in the α-Al matrix might weaken the regular reflections and spread out the distribution of scattering intensity, leading to broadened or multiple peaked diffraction lines [14].

The present study has evolved from earlier work [2, 3, 10, 11, 14]. It yields some detailed results which may elucidate the origin of inhomogeneities in rapidly

0022–2461

solidified Al–Cu and Al–Zn ribbons. X-ray diffraction, scanning and transmission electron microscopy have been employed to analyse the alloys.

2. Experimental procedure

Alloys of aluminium with 2.5, 4, 5 and 17.3 at % Cu and 4, 10, 26 and 40 at % Zn, respectively, were prepared from high-purity base metals. Ribbons with a thickness varying from 30 to 80 μm and a width of 4 mm were obtained using single copper roller melt-spinning in a protective argon atmosphere [11]. The temperature of the melts was selected at 800 °C, and the melts were ejected with an argon jet applying an overpressure of 20 kPa. The peripheral velocity of the wheel was 25 m s^{-1}. After preparation all Al–Zn ribbons were immediately stored in liquid nitrogen to prevent subsequent decomposition at room temperature.

The determination of lattice parameters and diffraction line profile analysis for the supersaturated α-Al matrix in the ribbons was performed with a Rigaku rotating anode (CuK_α) X-ray generator equipped with a Rad-B diffractometer (XRD). A step-scan data acquisition procedure was selected for this experiment with steps of 0.01° in 2θ and a sampling time of 5 s per step.

The composition, microstructure and precipitate distribution along cross-sections of these ribbons were examined by a Philips SEM505 scanning electron microscope (SEM) equipped with an X-ray energy-dispersive spectrometer (EDS) using a spot size of 1 μm. A Philips EM430 300 kV transmission electron microscope (TEM) combined with an EDAX 9900 energy-dispersive X-ray analysis system was employed to analyse the local solute content in the α-Al matrix of samples, using a spot size of ~1 nm. *In situ* precipitation processes in local regions of the ribbons were studied using a single tilt heating stage in a Philips CM20 200 kV TEM. Preparation of TEM samples from the wheel-side and top-side of the ribbons was done by single-side electropolishing in a Struers Tenupol twin immersion jet polishing apparatus at − 20 °C using an electrolyte of 25% nitric acid in methanol.

3. Results and analysis

The characteristic heterogeneous microstructure of the as-quenched ribbons with refined grains on the wheel-side followed by columnar and cellular zones towards the top-side can be seen in the Al–Cu alloys, while a uniform columnar structure is observed throughout the Al–Zn ribbons (Fig. 1). With increasing alloy concentration these structures become very fine, and the thickness of the ribbons decreases in both systems.

3.1. As-quenched samples

The equilibrium Θ phase is the only type of precipitate seen in the as-quenched Al–Cu alloys. They occur either in grain boundaries or in the Al matrix. SEM micrographs from longitudinal cross-sections of the Al–2.5 at % Cu ribbon show a non-uniform distribution of the Θ precipitates across the ribbon (Fig. 2a). In the wheel-side there is almost a single α-Al matrix containing a high density of dislocations and very few Θ precipitates (Fig. 2a and b). More Θ phase appears in the middle part and the top-side of the ribbon where it gradually becomes coarser (Fig. 2a and c). A similar morphology can also be seen in the Al–4 and 5 at % Cu alloys. For the eutectic Al–17.3 at % Cu ribbons the top-side exhibits a standard eutectic structure (Fig. 3a) with a mean dendrite arm spacing (DAS) about 90 nm. However, in the wheel-side a degenerate eutectic is the dominating microstructure (Fig. 3c). In addition, a very fine lamellar eutectic structure with DAS value from 40 to 50 nm surrounded by the degenerate eutectic is found in a few regions of the wheel-side (Fig. 3b).

Fig. 4 shows the profiles of X-ray diffraction lines from the α-Al phases in as-quenched Al–Cu alloys. A pronounced angle-dependent broadening of the reflections is obtained in all of the Al–Cu ribbons, e.g. from 0.45° for the (1 1 1) reflection to 0.78° for the (3 3 1) reflection in the Al–5 at % alloy. This broadening increases with increasing alloy concentration (Table I). The values for the line broadening in the present Al–Cu ribbons are much less than those quoted by Jansen [1], for instance, who obtained 1.2° for the (3 3 1) reflection. Furthermore, in three alloys with 2.5 to 5 at % Cu the lines are splitting into double peaks (Fig. 4).

In the low-concentrated Al–Zn (4 and 10 at %) alloys a single α-Al phase alone is formed, while for the two high-concentrated Al–Zn alloys the supersaturated α-Al matrix co-exists with minor amounts of fine β-Zn particles precipitated in the grain boundaries (Fig. 5). Furthermore, the α-Al grains consist of several sub-grains which are slightly misoriented and separated by small angle boundaries made up of dislocation arrays. The microstructure in these alloys is very uniform across the ribbons.

Broadening and splitting of the diffraction lines from the α-Al phase do not occur in the Al–4, 10 and 26 at % Zn alloys. The width of the diffraction lines in these alloys is only slightly larger than for pure aluminium (Table I). In contrast, for the Al–40 at % Zn alloy the diffraction lines from the α-Al phase are split into three peaks and show a significant broadening (Fig. 6).

The solute contents in the α-Al phases for all Al–Cu and Al–Zn alloys with either a single or multiple diffraction peaks are estimated from lattice parameter determinations (Table I) [7, 16]. EDAX analysis of the Al–2.5 at % Cu ribbon using the nanoprobe technique shows that the copper solute concentration in the α-Al matrix is about 2.6 at % in the wheel-side region and 1.2 at % in the top-side region. However, such compositional variations cannot be detected from the EDS analysis in the cross-section of all Al–Cu ribbons due to the larger spots size used which simultaneously covers the α-Al matrix and the Θ precipitates.

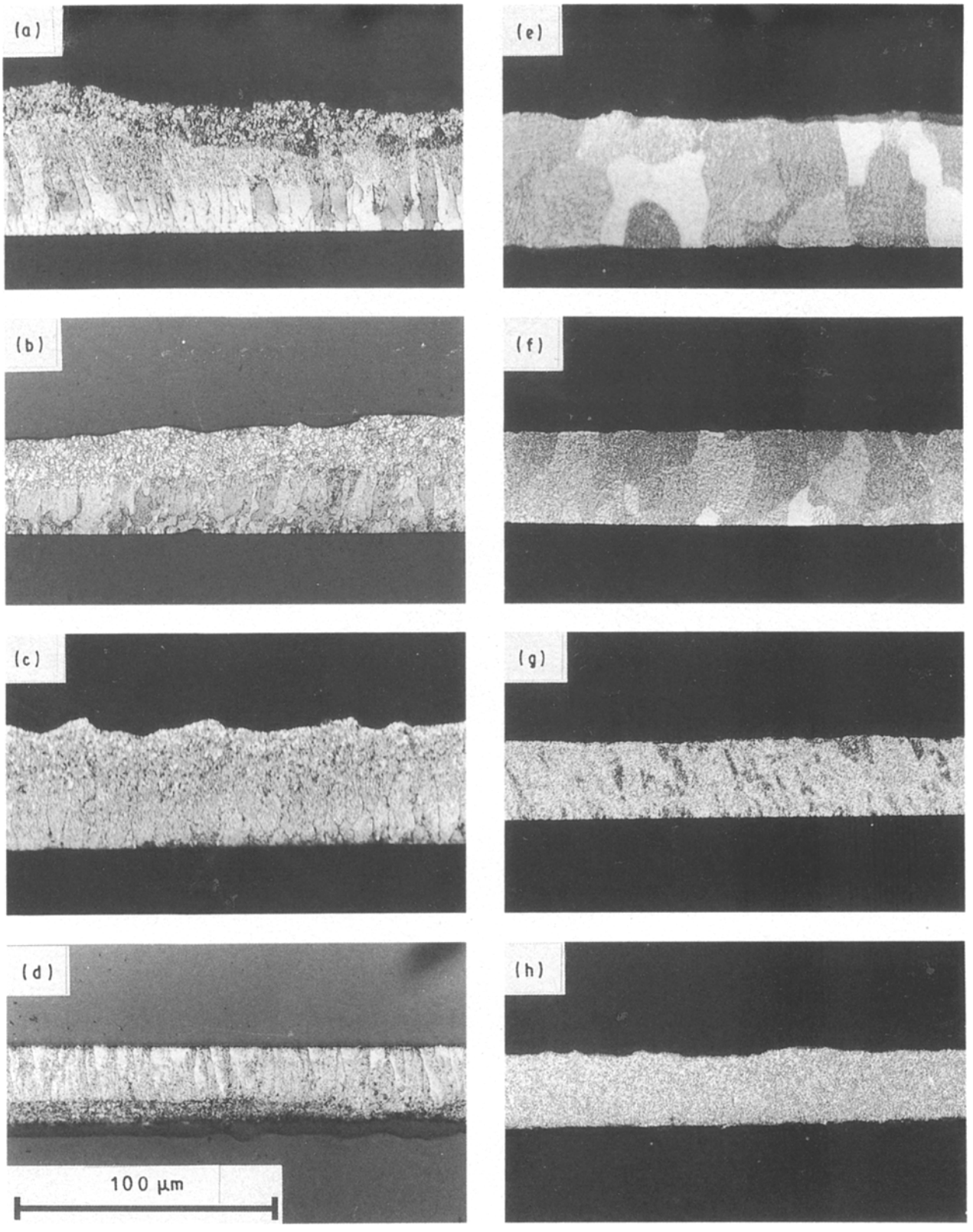

Figure 1 Optical micrographs showing microstructures along cross-sections of the as-quenched ribbons where the wheel-side is downward. (a–d) Al–2.5, 4, 5 and 17.3 at % Cu, respectively; (e–h) Al–4, 10, 26 and 40 at % Zn, respectively.

3.2. Annealed samples

Fig. 7a shows an example of the distribution of metastable Θ′ precipitates formed in a ribbon cross-section for the Al–Cu alloy after annealing. The density of Θ′ phase in the wheel-side area (Fig. 7b) is much higher than that in the top-side region (Fig. 7c). After further annealing this metastable phase finally transforms to the equilibrium Θ phase located inside the α-Al grains only (Fig. 8). There is no formation of Guinier–Preston (GP) zones and precipitation-free zones are not observed in any of the Al–Cu alloys during the precipitation processes. When the reaction of the Θ′ phase to the Θ phase is completed, the initial double peaks in the diffraction patterns are changed to

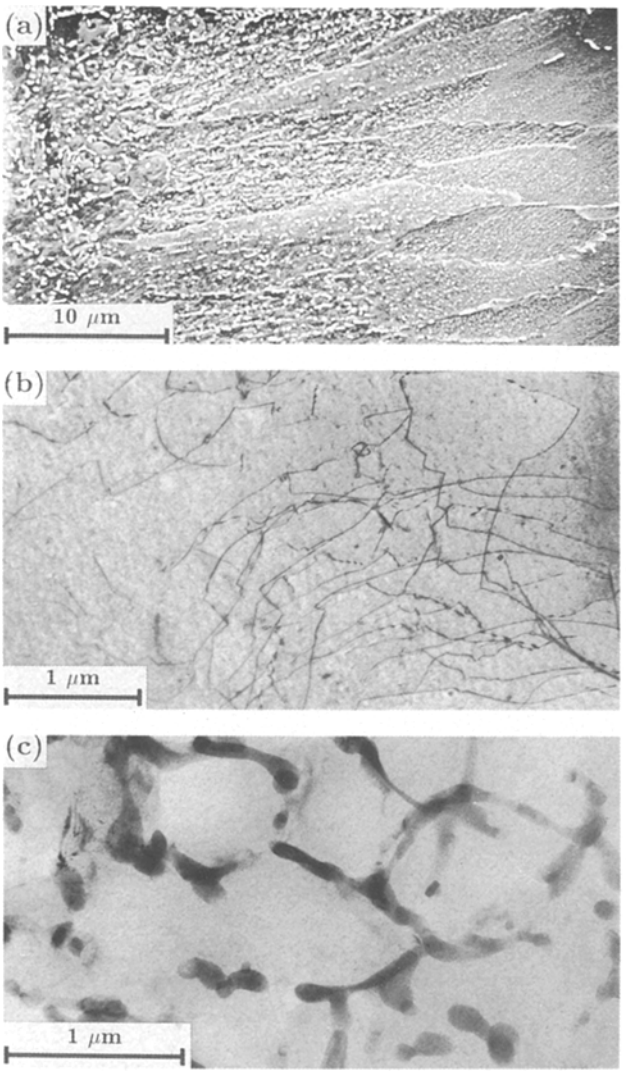

Figure 2 SEM and TEM micrographs illustrating the occurrence of inhomogeneous precipitation of the Θ phase in as-quenched Al–2.5 at % Cu ribbon. (a) SEM from a cross-section where the wheel-side is to the right; (b, c) TEM from the wheel-side and top-side, respectively.

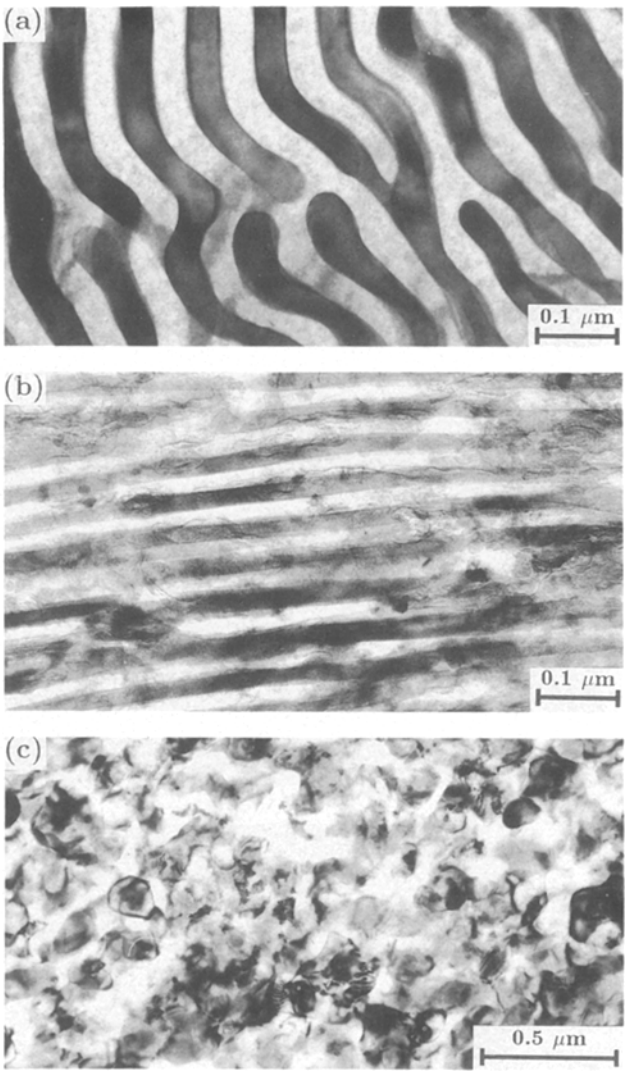

Figure 3 TEM micrographs from as-quenched Al–17.3 at % Cu ribbon. (a) Typical lamellar eutectic structure in the top-side; (b, c) fine lamellar eutectic and degenerate structures, respectively, in the wheel-side.

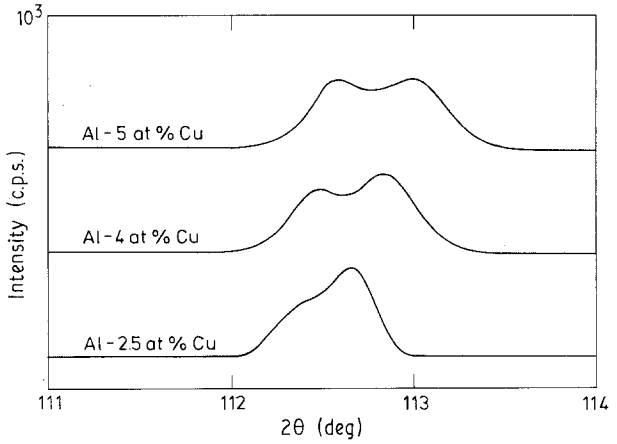

Figure 4 X-ray diffraction line profiles showing the appearance of doubly split peaks from the (3 3 1) reflection of as-quenched Al–2.5 to 5 at % Cu alloys.

TABLE I Solute contents (C) and X-ray diffraction line width (W) of the α-Al phases for as-quenched alloys

Alloy	C (at %)			W(deg θ)	
	c_1	c_2	c_3	(3 1 1)	(3 3 1)
Pure Al				0.362	0.360
Al–2.5 at % Cu	0.8	2.4			0.672
Al–4 at % Cu	1.1	3.7			0.738
Al–5 at % Cu	1.2	4.5			0.777
Al–17.3 at % Cu	5.7				0.840
Al–4 at % Zn	4.1			0.347	
Al–10 at % Zn	9.7			0.368	
Al–26 at % Zn	25.4			0.414	
Al–40 at % Zn	14.9	33.8	50.2	0.900	

a single peak with a width and a position approaching those of pure aluminium (Table II).

During annealing of the Al–Zn (4, 10 and 26 at %) alloys the precipitation sequence is as follows: supersaturated α-Al solution → GP zones → metastable R phase → equilibrium β-Zn phase. In contrast, the α-Al solid solution transforms discontinuously to the β-Zn phase during annealing of the Al–40 at % Zn alloy. The GP zones are homogeneously distributed in the Al matrix. Figs 9 and 10 demonstrate the evolution of

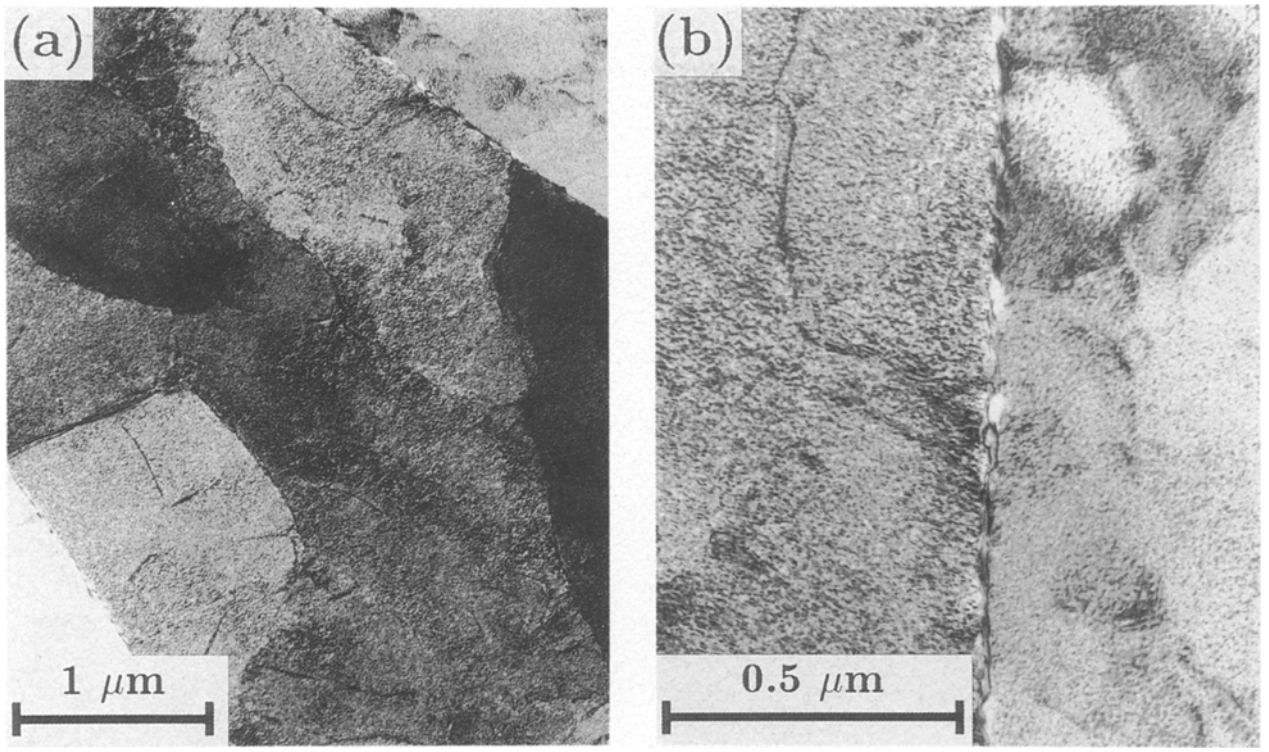

Figure 5 TEM micrographs from as-quenched Al–26 at % Zn alloy. (a) The α-Al phase with grain-boundary β-Zn precipitates and dislocation wall sub-grain boundaries; (b) enlargement showing grain-boundary β-Zn precipitates.

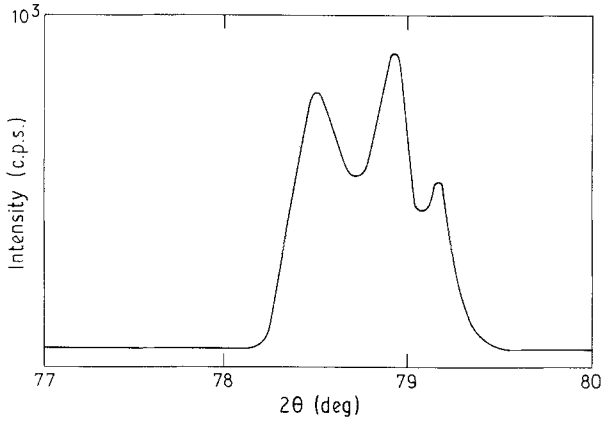

Figure 6 X-ray diffraction line profile showing the appearance of three split peaks from the (3 1 1) reflection of as-quenched Al–40 at % Zn alloy.

the various precipitates in an Al–26 at % Zn alloy. In agreement with the observation of Melton and Edington [17], there are two different mechanisms of nucleation for the R and the β-Zn phases. In most of the thick areas of the TEM foils, the R phase with a lamellar structure nucleates near the grain boundaries and gradually grows into the Al matrix containing the GP zones, where it will finally cover the entire matrix. When the GP zones are totally dissolved at higher temperature, the circular β-Zn precipitates begin to form in the regions of the R phase lamellae. The precipitation of the R/β phases is inhomogeneous in these regions. In thin areas near the hole edge of the samples, however, a large number of small platelets of the R phase will form homogeneously throughout the grains. After annealing at higher temperature they gradually transform to the β-Zn phase with a rhombic shape (Fig. 10). There is no evidence for the occurrence of precipitation-free zones in either case.

It is interesting to observe the changes of the diffraction line profiles from the α-Al phase in the annealed Al–Zn alloys. The triple peaks in the as-quenched Al–40 at % Zn alloy develop into a somewhat broadened single peak. For the two lower-concentrated Al–Zn (4 and 10 at %) alloys the diffraction lines are slightly broadened, while the single peak splits into a broadened double peak for the Al–26 at % Zn alloy (Fig. 11). After further annealing at higher temperature the double peak changes into a narrow single peak in the Al–26 at % Zn alloy, and in the three other alloys the line widths also decrease. Table II summarizes the widths of the (3 1 1) reflection and the solute concentration of the α-Al matrix calculated from the lattice parameters of these alloys [16]. Furthermore, point nanoprobe analysis for the Al–26 at % Zn alloy shows that the zinc solute content is about 10 at % in the α-Al phase between the lamellae of R phase, while it is anticipated to be nearly the same as the average alloy composition in areas containing GP zones [18].

4. Discussion

For the as-quenched Al–Cu ribbons, the inhomogeneities in the microstructure along the cross-sections result from the solidification arrest during quenching [9]. Fig. 12 shows a schematic solidification arrest in the cooling curve during rapid solidification. It consists of a nucleation undercooling stage (I) followed by

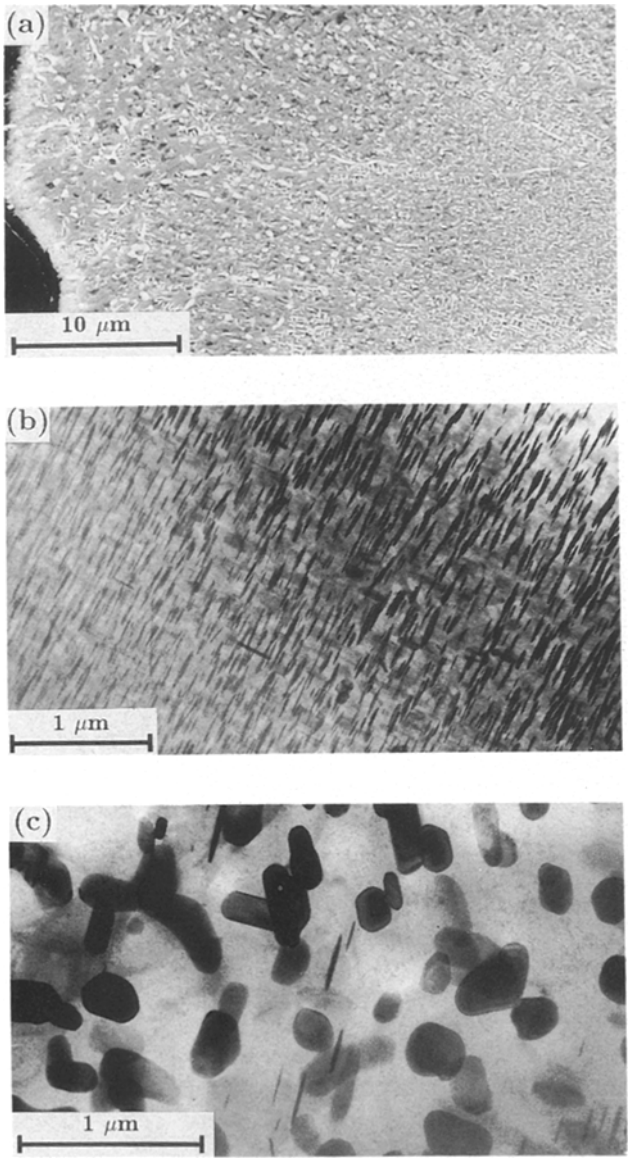

Figure 7 Occurrence of inhomogeneous precipitation of Θ′ platelets in Al–2.5 at % Cu alloy annealed at 280 °C. (a) Cross-section (SEM) where the wheel-side is to the right; (b) wheel-side (TEM) with a high density of Θ′ platelets; (c) top-side (TEM) with many Θ precipitates and very few Θ′ platelets.

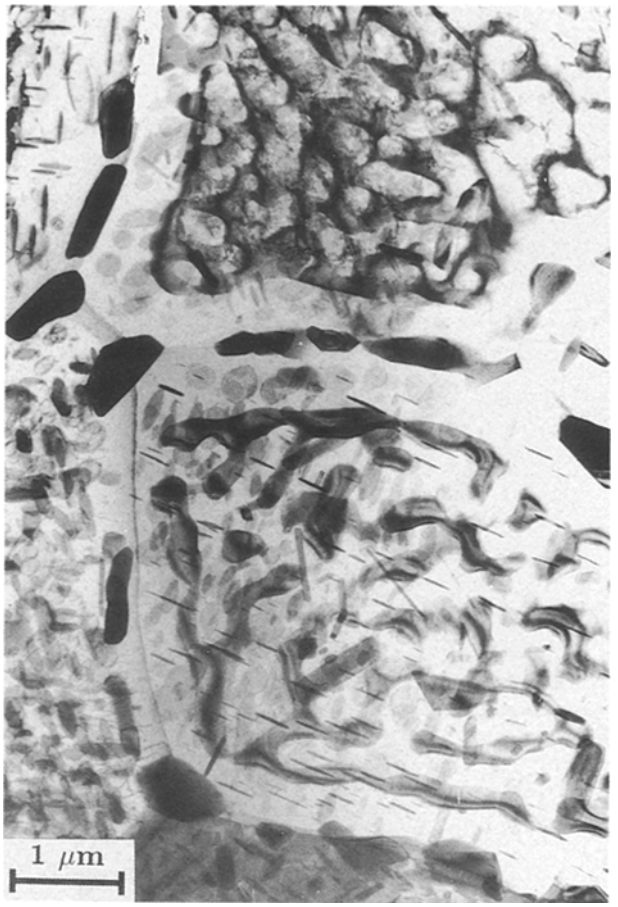

Figure 8 TEM micrograph from the wheel-side of Al–2.5 at % Cu ribbon annealed at 300 °C, showing the transformation of Θ′ to Θ inside the Al grains.

a recalescence stage (II) to a steady-state growth plateau (III). Thus, the local cooling rates are expected to be different in these stages. Taking the eutectic Al–Cu ribbon as an example and using the relationship between cooling rate and DAS value [19], the local cooling rates can be calculated to be about 6×10^5 °C s^{-1} in the wheel-side and about 1×10^5 °C s^{-1} in the top-side. Previous results [9, 20, 21] have indicated that the cooling rates at the onset of solidification are found to be approximately one order of magnitude higher than the mean cooling rates over the whole solidification range.

This difference in cooling rates not only leads to inhomogeneous microstructures but also to a non-uniform precipitation of the Θ phase along cross-sections of the as-quenched Al–Cu ribbons. Therefore, it is not surprising to find compositional variations on a macroscopic scale. The fact that we observe two α-Al phases with different compositions, rather than a continuous change of concentrations across the ribbons, seems to be associated with the three-stage cooling curve (Fig. 12), which is in itself related to the changes in microstructure across the ribbons [22]. The top-side with a cellular structure is nearly depleted of copper in supersaturated solution, and is nearly saturated with the stable Θ phase. On the other hand, in the regions with a columnar structure and in the chill zone at the wheel-side copper is retained in a strongly supersaturated solution. Indications of such compositional variations are supported by point nano-probe analysis from both regions of the Al–2.5 at % Cu ribbon. In fact, there is agreement between the solute contents determined by these analyses and those estimated from the lattice parameter of the α-Al phase in the wheel-side and top-side, respectively. This indicates that the double peaks in the diffraction lines can be associated with these two α-Al phases. As compared to earlier reports [2, 3], under identical processing conditions, these alloys do not show local compositional variations across grain boundaries, and hence precipitation-free zones are not expected. In addition, the variation in precipitation density of the Θ′ phase during annealing can be considered to be a result of these initial compositional differences.

The uniform microstructure and the formation of a single α-Al phase in all the as-quenched Al–Zn alloys show that variations in the cooling rate similar to those occurring in the Al–Cu alloys are suppressed

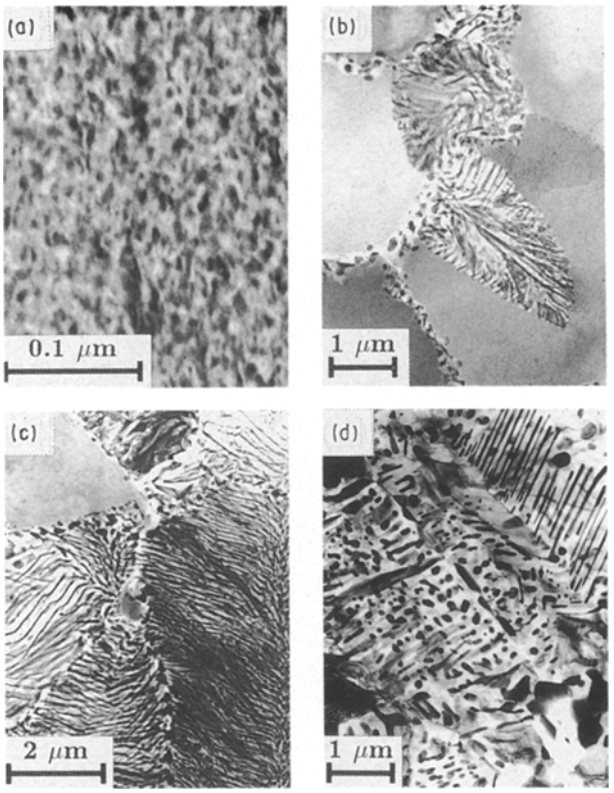

Figure 9 TEM micrographs taken during annealing from thick areas of Al–26 at % Zn foil. (a) GP zones at room temperature; (b) nucleation of R lamellar structure near grain boundaries. The R phase grows inhomogeneously into the Al matrix with GP zones at 80 °C; (c) nearly full transformation of R lamellae at 150 °C; (d) β-Zn phase precipitation at 200 °C.

due to a much higher extended solubility [23]. From the appearance of a single peak in the diffraction profiles the concentration of Al–4, 10 and 26 at % Zn alloys is believed to be homogeneous across the whole thickness of the ribbons, in agreement with the uniform morphology across the entire thickness of the ribbons. However, the triple peak in the Al–40 at % Zn alloy can be related to three isostructural f.c.c. modifications formed during quenching [24]. This is verified from the estimation of solute concentrations derived from the lattice parameters of these three peaks, and accordingly, the matrix compositions in this alloy vary in grains with different morphologies.

While formation of homogeneous distributions of small R platelets is only seen during annealing in the thin regions, the non-uniform precipitation of the R phase with a lamellar structure is the major observation in most areas of the annealed Al–26 at % Zn sample. Such non-uniform precipitation is due to the preferred nucleation of these lamellae in grain boundaries. With regard to the previous analysis [2, 3], the local solute concentration in as-quenched samples is initially high near the grain boundaries and lower in the Al matrix. Therefore, this preferred nucleation of the R phase in the Al–Zn alloys might originate from such compositional differences. On the other hand, inhomogeneous precipitation of the R phase leads to the co-existence of two α-Al phases with different solute contents. The Al matrix between the lamellae of the R phase contains less zinc in solution than the Al

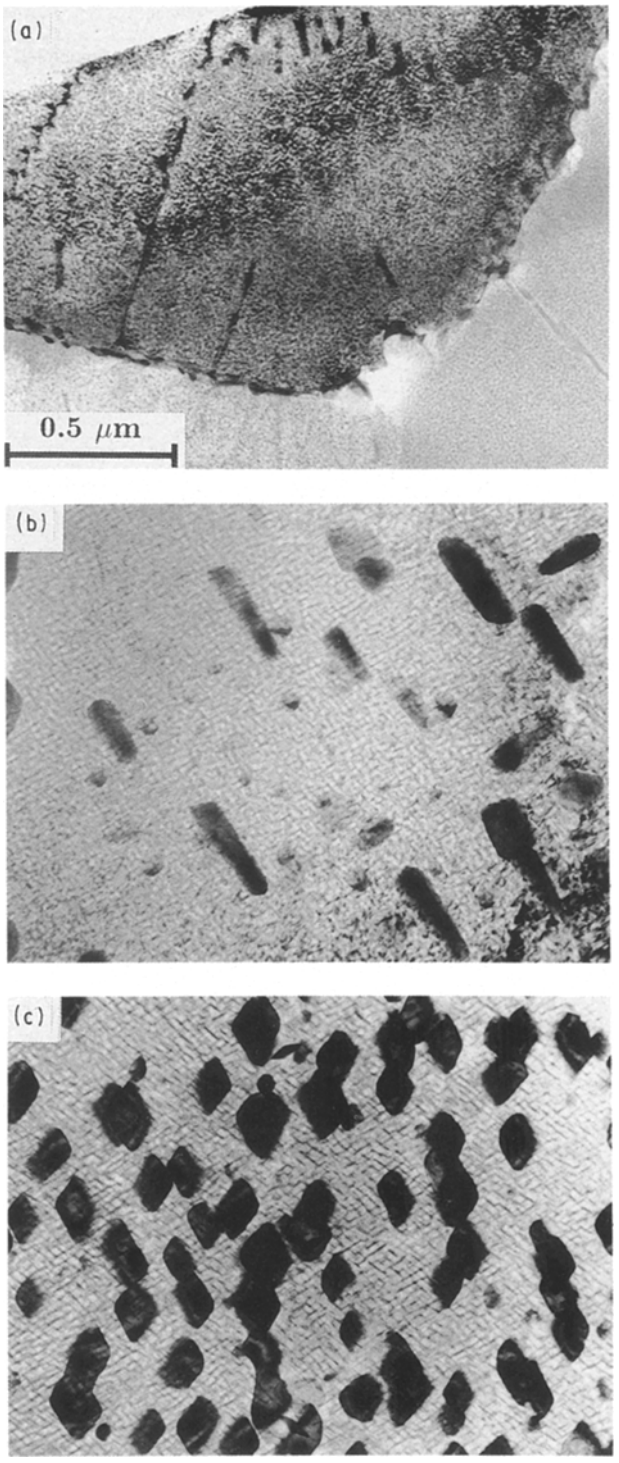

Figure 10 TEM micrographs taken during annealing from thin areas of Al–26 at % Zn foil. (a) GP zones at room temperature; (b) homogeneous nucleation and growth of small R platelets inside α-Al grains at 160 °C; (c) rhombic β-Zn phase at 200 °C with retained R phase in the background.

matrix still containing a high density of GP zones. The solute solubilities of these two phases detected by nanoprobe analysis are comparable to those derived from lattice parameter determinations of the respective double diffraction peaks. These analyses indicate that the kinetics associated with double-peaked diffraction lines in the Al–Zn alloys is different from the kinetics associated with formation of precipitation-free zones [10, 15]. Furthermore, the occurrence of double diffraction peaks can only be associated with a partial and non-uniform precipitation of the R phase

TABLE II Solute contents (C) and X-ray diffraction line width (W) of the α-Al phases for annealed alloys

Alloy	Annealing		C (at %)		W (deg 2θ)	
	Temperature (°C)	Time (h)	c_1	c_2	(3 1 1)	(3 3 1)
Al–2.5 at % Cu	280	0.5				0.420
Al–4 at % Cu	260	0.5				0.412
Al–5 at % Cu	260	0.5				0.420
Al–17.3 at % Cu	220	0.5				0.418
Al–4 at % Zn	110	1	3.8		0.410	
	160	24	3.5		0.373	
Al–10 at % Zn	110	1	8.1		0.444	
	160	0.5	7.2		0.478	
	160	24	4.4		0.395	
Al–26 at % Zn	110	0.5	9.6	25.1	0.774	
	160	0.5	3.9		0.414	
Al–40 at % Zn	110	0.5	7.8		0.882	
	160	0.5	4.2		0.378	

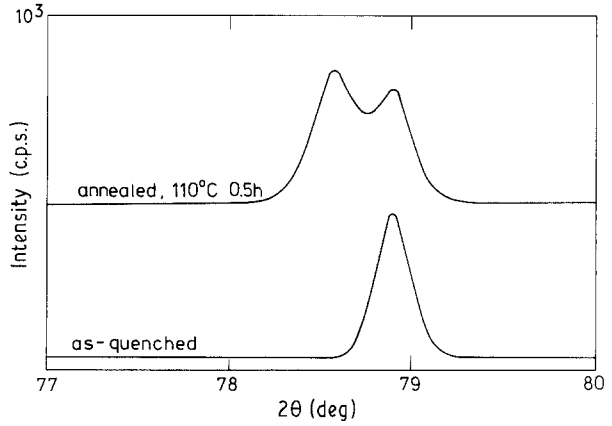

Figure 11 X-ray diffraction line profiles, showing the appearance of double peaks from the (3 1 1) reflection of annealed Al–26 at % Zn alloy.

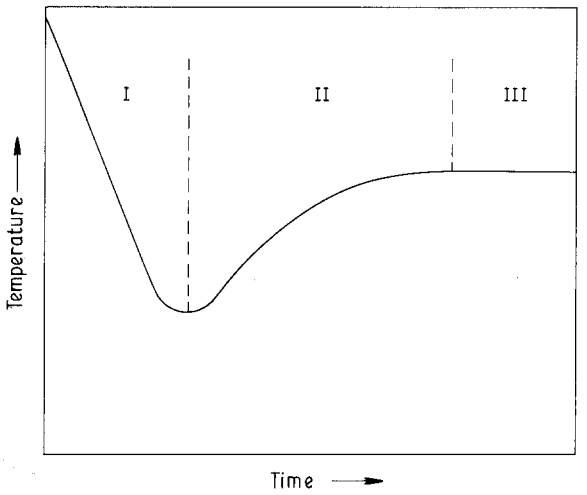

Figure 12 Schematic illustration showing the effect of solidification arrest on the cooling curve during rapid solidification. The cooling sequence contains three stages: (I) nucleation undercooling, followed by (II) recalescence, and (III) termination in a steady-state growth plateau.

with lamellar structure, where considerable amounts of the GP zones are retained in the same grains. This partial and non-uniform precipitation has also been reported to be a necessary requirement during annealing of Al–Mg ribbons [10]. Annealing for a long time or at high temperature will lead to merging of the split peaks into a single peak as a result of complete formation of the R phase or the β-Zn phase.

The retention of single diffraction lines from the low-concentrated Al–Zn alloys after annealing may suggest either that the GP zones are easily dissolved, or that the amount of R precipitates is too low to deplete the α-Al matrix of zinc to an extent which will lead to formation of split peaks. Annealing of the Al–40 at % Zn alloy is associated with disappearance of the three Al phases and the formation of β-Zn precipitates, combined with development of an α-Al phase with uniform composition. This is deduced from the change of the triple peak into a single diffraction line.

In the present investigation, the appearance of broadened diffraction lines from the α-Al phase may be ascribed partly to non-uniform accumulation of microstrains [14] formed during quenching of the Al–Cu alloys, and during the precipitation process in the Al–Zn alloys, respectively. The compositional variations resulting from the different solidification rates are responsible for this heterogeneous distribution of quenched-in stresses [4, 25]. In addition, the inhomogeneous precipitation of coherent or semi-coherent phases can cause a different degree of strain misfit between these phases and the Al matrix [10]. This can explain why the widths of the diffraction lines increase with increasing solute concentration or with increasing cooling rate [1, 2]. Such broadening is strongly dependent on the amount, size and type of the precipitates which in itself depends on the annealing temperature and time. If these coherent precipitates are totally transformed to non-coherent phases, the strains are released and the width of the diffraction lines will approach those of pure aluminium. A good explanation and comparison for these have been given in different compositions of as-quenched and annealed Al–Mg alloys [4, 10, 25].

5. Conclusions

1. In as-quenched Al–Cu alloys, the heterogeneous microstructure, compositional variation and non-uniform precipitation of the equilibrium Θ phase originate from differences in the local cooling rates due to solidification arrest and recalescence. The initial variations in composition lead to inhomogeneous precipitation of the metastable Θ′ phase during subsequent annealing. In Al–Zn alloys non-uniform precipitation of the metastable R phase during annealing may arise from preferable nucleation near the grain boundaries.

2. In these two alloy systems, the occurrence of double or triple-peaked X-ray diffraction lines from the α-Al matrix can be ascribed to compositional variations. Precipitation-free zones in the vicinity of grain boundaries do not develop in the present Al–Cu and Al–Zn ribbons.

3. The double-peaked diffraction lines in three as-quenched Al–Cu ribbons result from two α-Al solutions with high solute solubility in the wheel-side and with low solute solubility in the top-side, respectively.

4. For the as-quenched Al–40 at % Zn alloy the composition varies from grain to grain in three isostructural f.c.c. modifications which are responsible for the three split diffraction peaks. Appearance of the double diffraction peaks in the annealed Al–26 at % Zn alloy is associated with two α-Al phases with different solute concentrations: the low concentration is located between the lamellae of the R phase, while the regions with GP zones retained represent the high concentration.

Acknowledgements

Nanoprobe analysis was performed by A. Henschel (Department of Applied Physics, Technical University of Denmark). SEM was performed by I. Søndergård (Department of Metallurgy, Technical University of Denmark). Financial support from The Danish Natural Science Research Council and The Daloon Foundation is greatfully acknowledged.

References

1. C. JANSEN, PhD Thesis, MIT, Cambridge, Massachusetts (1971).
2. D. B. WILLIAMS and J. W. EDINGTON, in "Rapidly Quenched Metals", edited by N. J. Grant and B. J. Giessen (MIT Press, Cambridge, Massachusetts, 1976) p. 135.
3. L. J. MASUR and M. C. FLEMINGS, in "Rapidly Quenched Metals", edited by T. Masumoto and K. Suzuki (Japan Institute of Metals, Sendai, 1982) p. 1557.
4. J. A. van der HOEVEN, P. van MOURIK and E. J. MITTEMEIJER, *J. Mater Sci. Lett.* **2** (1983) 158.
5. S. PAIDASSI and J. CHEVRIER, in "Rapidly Quenched Metals", edited by S. Steeb and H. Warlimont (North-Holland, Amsterdam, 1985) p. 957.
6. M. H. BURDEN and H. JONES, *J. Inst. Metals* **98** (1970) 249.
7. P. H. SHINGU and R. OZAKI, *Sci. Rep. RITU A* (June 1978) 21.
8. K. EMMERICH, in "Rapidly Quenched Metals", edited by S. Steeb and H. Warlimont (North-Holland, Amsterdam, 1985) p. 71.
9. B. CANTOR, in "Science and Technology of the Undercooled Melt", edited by P. R. Sahm, H. Jones and C. M. Adam (M. Nijhoff, Dordrecht, 1986) p. 3 and references therein.
10. P. van MOURIK, "Ageing of Liquid-Quenched and Solid-Quenched Aluminium Base Alloys; Analysis of Lattice-Parameter Variations", doctoral thesis, Delft University (1988) p. 77.
11. Q. LI, E. JOHNSON, A. JOHANSEN and L. SARHOLT-KRISTENSEN, in Proceedings of International Conference on Light Metals, edited by T. Khan and G. Effenberg (ASM European Council, 1990) p. 349.
12. M. A. R. WEILL, *Rev. Métall.* **49** (1950) 364.
13. E. C. W. PERRYMAN, *Acta Metall.* **3** (1955) 412.
14. M. J. GITGARTS and V. I. KOMARAVA, *Phys. Met. Metall.* **53** (1982) 170.
15. D. B. WILLIAMS and E. P. BUTLER, *Int. Met. Rev.* **26** (1981) 153.
16. J. L. MURRAY, *Bull. Alloy Phase Diag.* **4** (1983) 55.
17. K. N. MELTON and J. W. EDINGTON, *J. Mater. Sci.* **9** (1974) 543.
18. T. R. ANANTHARAMAN, V. RAMASWAMY and E. P. BUTLER, *ibid.* **9** (1974) 240.
19. M. H. BURDEN and H. JONES, *J. Inst. Metals* **98** (1970) 249.
20. D. R. HARBUR, J. W. ANDERSON and W. J. MARAMAN, *TMS-AIME* **245** (1969) 1055.
21. M. J. TENWICK and H. A. DAVIES, in "Rapidly Quenched Metals", edited by S. Steeb and H. Warlimont (North-Holland, Amsterdam, 1985) p. 67.
22. B. CANTER, W. T. KIM, B. P. BEWLAY and A. G. GILLEN, *J. Mater. Sci.* **26** (1991) 1266.
23. I. V. SALLI and L. P. LIMINA, in "Growth and Imperfections in Metallic Crystals", edited by D. E. Ovsienko (Consultants Bureau, New York, 1968) p. 251.
24. T. R. ANANTHARAMAN and K. G. SATYANARAYANA, *Scripta Metall.* **7** (1973) 189.
25. P. van MOURIK, E. J. MITTEMEIJIER and Th. H. de KEIJSER, *J. Mater. Sci.* **18** (1983) 2706.

Received 9 August 1991
and accepted 7 April 1992